Impedance Spectroscopy of Self-Assembled Monolayers on Au(111): Sodium Ferrocyanide Charge Transfer at Modified Electrodes

Richard P. Janek and W. Ronald Fawcett*

Department of Chemistry, University of California, Davis, Davis, California 95616

Abraham Ulman

Department of Chemistry, Brooklyn Polytechnic University, Brooklyn, New York 11202

Received August 29, 1997. In Final Form: March 6, 1998

The Faradaic impedance of a Au(111) electrode modified by three different self-assembled monolayers has been studied over a wide frequency range in aqueous $NaClO_4$ solutions in the presence of 1 mM $[Fe(CN)_6]^{4-/3-}$. The impedance characteristics of the bare electrode are compared with those of the same electrode modified with decanethiol, ω-hydroxydecanethiol, and 4′-hydroxy-4-mercaptobiphenyl. The 4′-hydroxy-4-mercaptobiphenyl molecule is susceptible to $\pi-\pi$ interactions and is of special interest as a mediator of electron transfer. In the case of the decanethiol and ω-hydroxydecanethiol systems the interfacial impedance can be modeled by the Randles circuit. However, for the 4′-hydroxy-4-mercaptobiphenyl system, the impedance behavior is more complex with a resistance in the monolayer parallel to and distinguishable from the expected Faradaic impedance. This behavior is quite different from that discussed to date in the literature and assumed in the interpretation of voltammetric data for modified electrodes. The parameters for these systems are reported here as a function of the type of electrode modification. The consequences of the present observations are discussed with respect to the phenomena observed.

Introduction

The dynamics of charge transfer at the electrochemical interface are strongly influenced by the nature of the electrode surface and the structure of the electrical double layer.[1,2] Recent studies of electrodes modified by self-assembled monolayers (SAMs)[3−5] have shown that electron transfer to a species in solution is retarded either by reducing the active area of the electrode or by preventing the redox species from approaching the electrode closely. This phenomenon has been exploited to measure the charge-transfer kinetics of fast reactions which are difficult to observe on bare metal electrodes because the reaction is diffusion-limited over most of the polarizable range of the electrode.[5] In addition, inhibition of electron transfer at metal surfaces is a major concern in efforts to prevent corrosion and information garnered in fundamental studies of these systems can be applied to this important engineering problem. The impedance of an electrode undergoing heterogeneous electron transfer is usually described on the basis of the model by Randles.[6,7] This model is often readily applied to a diverse collection of experimental systems, some of which involve SAMs.[8] The present study seeks to test the Randles hypothesis over a range of electrochemical situations involving self-assembled monolayers using the adsorbates shown in Scheme 1.

Scheme 1. Schematic Illustration of SAMs under Consideration in This Study with (A) Bare Au(111), (B) Au(111) Modified with Decanethiol (DT), (C) Au(111) Modified with ω-Hydroxydecanethiol (HDT), and (D) Au(111) Modified with 4′-Hydroxy-4-mercaptobiphenyl (HMB)

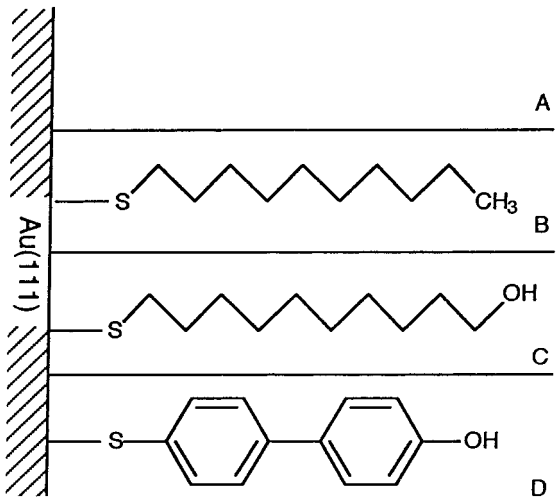

Heterogeneous electron transfer has been studied previously[3−5,8,20] in systems with self-assembled monolayers. The focus of much of this work has been to understand the influence of the surrounding medium on the dynamics of electron transfer as well as the role played by electronic coupling between the metal electrode and the redox system in solution on the rate constant to test fundamental theories. Ferrocene-terminated alkanethiol

(1) Delahay, P. *Double Layer and Electrode Kinetics*; Interscience Publishers and John Wiley and Sons: New York, 1965.
(2) Fawcett, W. R.; Opallo, M. *Angew. Chem., Int. Ed. Engl.* **1994**, *33* (21), 2131−2143.
(3) Miller, C. J.; Cuendet, P.; Gratzel, M. *J. Phys. Chem.* **1991**, *95*, 877−886.
(4) Finklea, H. O.; Snider, D. A.; Fedyk, J. *Langmuir* **1993**, *9*, 3660−3667.
(5) Chidsey, C. E. D. *Science* **1991**, *251*, 919−922.
(6) Randles, J. E. B. *Discuss. Faraday Soc.* **1947**, *1*, 11.
(7) Sluyters-Rehbach, M.; Sluyters, J. H. In *Comprehensive Treatese of Electrochemistry*; Yeager, E., Bockris, J. O'M., Conway, B. E., Eds.; Plenum Publishing: New York, 1984; pp 177−291.
(8) Sabatani, E.; Cohen-Boulakia, J.; Bruening, M.; Rubinstein, I. *Langmuir* **1993**, *9*, 2974−2981.

S0743-7463(97)00980-3 CCC: $15.00
Published on Web 05/02/1998

monolayers and unmodified thiols in the presence of solution-phase ferrocene, ferrocyanide, and other redox couples have been studied.[3−5] Common techniques used are potential step chronoamperometry (CA) and cyclic voltammetry (CV). However, the current−potential transients in CA are often complex due to double-layer charging and changes in monolayer charge density during the electron-transfer reaction. The effects of these interfacial parameters are not directly observed in these experiments. Impedance spectroscopy has an advantage over CA and CV because the effects of solution resistance, double-layer charging, and currents due to diffusion or to other processes occurring in the SAM are observed more explicitly. Therefore, in an effort to circumvent these problems, impedance spectroscopy has been applied in this study to systems involving SAMs.

If the electron-transfer reaction takes place at bare spots on the electrode surface, the fractional coverage may be estimated by comparing the charge-transfer resistance of the modified surface with the charge-transfer resistance of Au(111) without modification. Some discussion in the literature[4] concerns how the electron-transfer reaction takes place, that is, either via tunneling through the dielectric material of the SAM or via reaction pathways involving pores. In this study we also investigate the discrepancies[4,20] present in the various methods used to estimate the fractional coverage of the electrode by the SAM.

Theory

The interface is modeled as a collection of ideal circuit elements in the impedance spectroscopy experiment, including namely one of the most common circuits, that described by Randles. In the Randles circuit, it is assumed that the resistance to charge transfer and the diffusion impedance are both in parallel to the interfacial capacity. This parallel combination of R and C gives rise to a semicircle in the complex plane plot of $-Z''$ against Z'. The mass-transfer term, which cannot be represented by classical circuit elements (Warburg impedance), is observed as a low-frequency spur with a slope of unity.

Impedance spectroscopy[9] (IS) allows one to observe the magnitude of the interfacial electrical circuit elements and the pattern of interconnectivity of these ideal elements at a higher resolution than that for measurements based on cyclic voltammetry or chronoamperometry. It provides an excellent method to test the equivalent circuit model used to describe SAMs and charge-transfer reactions. A small-amplitude sinusoidal signal is applied to the electrochemical cell, and the current response is measured under potentiostatic control. The impedance

$$Z(j\omega) = \frac{\dot{V}(j\omega)}{\dot{J}(j\omega)} = Z'(\omega) + jZ''(\omega) \qquad (1)$$

is calculated as the ratio of the system voltage phasor, $\dot{V}(j\omega)$, to the current phasor, $\dot{I}(j\omega)$, which are generated by a frequency response analyzer during the experiment. $Z(j\omega)$ is a complex quantity ($j = \sqrt{-1}$) and is a function of the excitation angular frequency ω. Z' and Z'' can be calculated given an equivalent circuit model for the system using traditional algebraic methods of circuit analysis.[10]

(9) *Impedance Spectroscopy: Emphasizing Solid Materials and Systems*; Macdonald, J. R., Ed.; John Wiley & Sons: New York, 1987.
(10) Jordan, D. W.; Smith, P. *Mathematical Techniques: An introduction for the engineering, physical, and mathematical sciences;* Oxford University Press: Oxford, 1994; p 323.

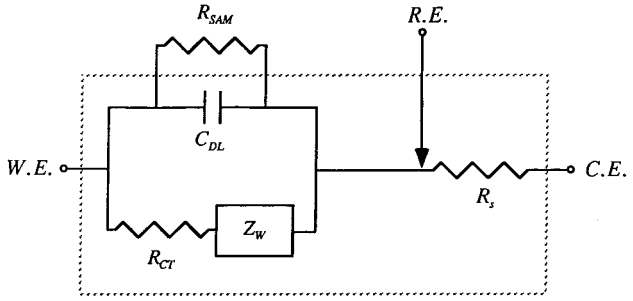

Figure 1. General equivalent circuit model used to obtain equations for Z' and $-Z''$. The CNLS regression results are shown in Table 1. W.E. is the working electrode, R.E. is the saturated calomel reference electrode, and C.E. is the gold leaf counter electrode. The dotted box encloses the traditional Randles circuit. The extra resistance, R_{SAM}, was only found for the HMB system.

Figure 1 shows a schematic diagram for the ideal circuit used to describe the observations in this study. The Randles term is represented by the conduction path between the working electrode and the counter electrode with the following elements in between: C_{DL}, R_{CT}, Z_W, and R_S, as shown in Figure 1 within the dotted box. C_{DL} is the double-layer capacitance, R_{CT} is the charge-transfer resistance, Z_W is the impedance due to mass transfer of the redox species to the electrode described by Warburg, and R_S is the solution resistance. If this circuit is valid, then

$$Z'_{\text{Randles}} = R_S + \frac{R_{CT} + \sigma\omega^{-1/2}}{(C_{DL}\sigma\omega^{1/2} + 1)^2 + \omega^2 C_{DL}^2 (R_{CT} + \sigma\omega^{-1/2})^2} \qquad (2)$$

and

$$Z''_{\text{Randles}} = \frac{\omega C_{DL}(R_{CT} + \sigma\omega^{-1/2})^2 + \sigma\omega^{-1/2}(\omega_{1/2} C_{DL}\sigma + 1)}{(C_{DL}\sigma\omega^{1/2} + 1)^2 + \omega^2 C_{DL}^2 (R_{CT} + \sigma\omega^{-1/2})^2} \qquad (3)$$

where

$$Z_w = \sigma\omega^{-1/2}(1 - j) \qquad (4)$$

In terms of microscopic parameters

$$R_{CT} = \frac{RT}{nFi_0} \qquad (5)$$

and

$$\sigma = \frac{RT}{n^2F^2A\sqrt{2}}\left(\frac{1}{D_O^{1/2}C_O^*} + \frac{1}{D_R^{1/2}C_R^*}\right) \qquad (6)$$

where R, T, n, and F have their usual meanings. A is the area of the electrode, D_i is the diffusion coefficient, and C_i^* is the bulk concentration of redox species i. i_0 is the exchange current density and is directly related to the rate constant for electron transfer. This work shows that a monolayer-dependent resistive term, R_{SAM}, in parallel with the Faradaic impedance of the interface is required to model accurately the impedance of certain SAM−electrode systems. A complete electrochemical description of the interface is achieved by measuring the impedance as a function of frequency, redox species concentration, and electrode potential. In addition to refining the equivalent circuit model which is necessary to analyze properly

these systems, this work also explores the electron-transfer properties of a novel class of SAMs: biphenylthiol films.

Experimental Section

Chemicals. Decanethiol (DT) was obtained from Aldrich and used as received. ω-Hydroxydecanethiol (HDT) was synthesized from 10-bromodecanol (Aldrich) by refluxing in 90% ethanol (Quantum Chemical)/water with 1.2 equiv of thiourea (Aldrich) for 5 h. The ethanol was removed by rotary evaporation. Then, 1.2 equiv of NaOH was added to hydrolyze the thiouronium salt in situ followed by a 30 min reflux. The reaction mixture was then extracted three times with chloroform (Aldrich). The crude product was separated on a silica gel (Baker) column with 5% ethyl acetate (Aldrich) in chloroform as the mobile phase with detection by TLC (with iodine development the large spot in the center of the plate was used). The final product was a slightly yellow viscous liquid at room temperature and gave a yield of 46%. Elemental analysis, ^{1}H NMR, and ^{13}C NMR gave the following results. Expected C, 63.01; H, 11.65; S, 16.84. Found: C, 62.95; H, 11.71; S, 15.21.

4′-Hydroxy-4-mercaptobiphenyl (HMB) was prepared by palladium-assisted coupling of 4-methylthiophenylmagnesium bromide and 4-iodoanisol. Thus, the $Pd(PPh_3)_4$ catalyst (0.2 mmol, Aldrich) was added to 4.68 g (20 mmol) 4-iodoanisol (Aldrich) in 5 mL of absolute THF (Aldrich), and the solution was brought to gentle reflux under dry nitrogen. A Grignard solution, prepared in the usual way from 1-bromo-4-methylthiobenzene (4.06 g, 20 mmol, Aldrich) and magnesium (22 mg-atom, Kodak) in 25 mL of THF, was transferred to the boiling 4-iodoanisol solution using a $^1/_8$-in. Teflon tubing. The entire system was under nitrogen, and nitrogen pressure was used to control the addition rate. The reaction was exothermic. First, the solution became clear, and then magnesium salts started to deposit. After the addition was completed, the mixture was refluxed for an additional 30 min. After cooling, the reaction mixture was poured into ice water (100 mL) containing 5 mL of HCl. The solid was filtered, washed with water, dried, and crystallized from heptane with some 2-propanol. The yield was 68%.

4-Methoxy-4′-methylthiobiphenyl (3.06 g, 20 mmol) was dissolved in 30 mL of dry DMF (Aldrich) under a nitrogen blanket. C_2H_5SK (4.6 g, 50 mmol) was added to the stirred solution, and it was refluxed gently for 6 h. After cooling, the solution was poured into ice water (100 mL) containing 5 mL of HCl. The solid was collected, washed with cold water, air-dried, and crystallized from heptane/2-propanol. The yield of 4′-hydroxy-4-mercaptobiphenyl was 78%. The structure was confirmed by ^{1}H NMR and ^{13}C NMR.

Sodium perchlorate was obtained from Fluka and used as received. Sodium ferricyanide and sodium ferrocyanide were used as received from Matheson Coleman & Bell. Nanopure water was obtained from a Barnstead filter system and had a resistivity of ~18 MΩ cm.

Electrochemical Cell and Instrumentation. A conventional three-electrode cell was used with a water jacket for temperature control and a Teflon stopper with holes for electrode insertion and a pure N_2 gas purge. All experiments were conducted at 25 ± 1 °C. The cell was enclosed in a grounded Faraday cage. A reference electrode was constructed by sealing a pure Ag wire into a glass tube with a solution of 0.01 M $AgClO_4$ and capped with a Vycor tip (stable after equilibration, −0.432 V vs SCE). The reference electrode was always isolated from the cell by a Luggin capillary containing the electrolyte. The $AgClO_4$ reference electrode was used because $KClO_4$ has a limited solubility and would precipitate in the liquid junction of a saturated calomel electrode. The counter electrode was a large area pure gold leaf. Impedance was measured with a Solartron 1255 frequency response analyzer (FRA) interfaced to an EG&G 283 potentiostat/galvanostat. The data acquisition and control was handled by a Zenith 286 PC interfaced to the FRA and the potentiostat via an IEEE-488 General Purpose Interface Bus (GPIB) and with software written in the C language in the DOS system. The instrument was thoroughly calibrated using the method of Sluyters et al.[11,12] by measuring the impedance of a collection of circuits composed of high-quality resistors and capacitors. Wave forms were monitored by an Iwatsu DS-6121 digital oscilloscope during data acquisition to ensure good signal quality. All glassware was cleaned by boiling in 50% HNO_4 for several hours and rinsed well with Nanopure water before use.

Procedure. The single-crystal (111 face) gold working electrode, obtained from Metal Crystals and Oxides LTD, Cambridge, England, was prepared by polishing. The following procedure was used: hand polishing on silicon carbide P4000 grinding paper, followed by a Buehler Ecomet 3 motorized wheel using wet alumina powder of finer and finer grades (from 3 μm down to 0.05 μm) on different felts according to Hamelin.[13] Once the surface of the electrode was observed to be defect free under 30× magnification, the electrode was rinsed in water and cycled from −0.5 to 1.4 V versus SCE in 0.01 M $HClO_4$ at 50 mV s^{-1} until a stable baseline was obtained. The geometric area of the electrode was 0.0856 cm^2. The "true" area of the electrode was estimated by measuring the charge corresponding to the reduction of gold oxide after electrolysis at 1.5 V versus SCE for 100 s.[14] A "roughness factor" of 1.65 was found for this electrode. All current densities and impedances are reported here with respect to the *geometric* area. Electrode modification was conducted by dipping overnight in 30 mM ethanolic solutions of thiol at room temperature followed by rinsing in clean ethanol (5 min) and then Nanopure water (5 min). The electrode was transferred to the cell, using the hanging meniscus solution contact technique, for impedance measurements. The concentration of sodium ferricyanide was equal to the concentration of sodium ferrocyanide and was 1 mM for all impedance measurements. The concentration of supporting electrolyte was 0.5 M $NaClO_4$. After the experiment, the electrode was rinsed, placed in a Bunsen flame, and quenched in Nanopure water to remove the SAM. The Au(111) baseline, in 0.01 M $HClO_4$, was obtained before modification and after the electrode had been flame treated to remove the SAM following the measurement. The electrode was stored in Nanopure water when not in use. The impedance measurements were performed at the formal potential of the $Na_3Fe(CN)_6/Na_4Fe(CN)_6$ couple, determined by cyclic voltammetry with an applied bias voltage of 0.230 V versus SCE (generated by the potentiostat), a 5-mV (rms) sinusoidal excitation amplitude, and an automatic analyzer integration time (0.001% SD of $\dot{I}(j\omega)$ correlator output) with a 100-s cutoff time, and measurements were made five times at each frequency and averaged during the run. The impedance was measured for 50 harmonic frequencies from 1 Hz to 10 kHz at 10 steps per decade. Each experiment was performed five times from modification to annealing, and the results were averaged. The impedance data were fit to an equivalent circuit model in the complex plane by using an algorithm based on that of Macdonald.[9] Both $-Z''$ and Z' data were used in the impedance fit (at the same time) by complex nonlinear regression (CNLS), which included analytic first derivatives of the trial function and the Levenberg−Marquardt algorithm.[15]

Results and Discussion

Cyclic Voltammetry. One of the advantages of working with single-crystal electrodes is that all experiments are performed on the same surface, which can be repeatedly cleaned and brought to the same initial conditions for each measurement. The cleanliness of the Au(111) surface is particularly evident by cyclic voltammetry in 0.01 M $HClO_4$. Although there is no quantitative study of the relationship between surface defects and cyclic voltammetry in 0.01 M $HClO_4$, several important defects, such as surface roughness, are noticeable as minor aberrations in the cyclic voltammogram. The oxidation

(11) Bongenaar, C. P. M.; Sluyters-Rehbach, M.; Sluyters, J. H. *J. Electroanal. Chem.* **1980**, *109*, 23−39.

(12) Andreu, R.; Gonzalez-Arjona, D.; Dominguez, M.; Molero, M.; Roldan, E. *Electroanalysis* **1991**, *3*, 377−383.

(13) Hamelin, A. In *Modern Aspects of Electrochemistry*; Conway, B. E., White, R., Bockris, J. O'M., Eds.; Plenum Press: New York, 1985; No. 16, Chapter 1.

(14) Woods, R.; Rand, D. A. J. *J. Electroanal. Chem.* **1971**, *31*, 29−38.

(15) Vetterling, W. T., Flannery, B. P. Press, W. H., Teukolsky, S. A., *Numerical Recipes in C*, 2nd ed. Cambridge University Press: New York, 1992; p 656.

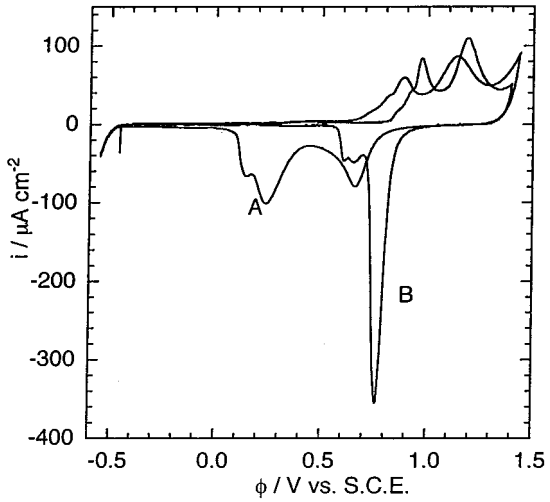

Figure 2. Cyclic voltammetry of Au(111) in (A) 0.01 M $NaClO_4$ and (B) 0.01 M $HClO_4$ at 50 mV s^{-1} from −0.5 V versus SCE to 1.45 V versus SCE: initial potential, −0.5 V; sweep direction, positive.

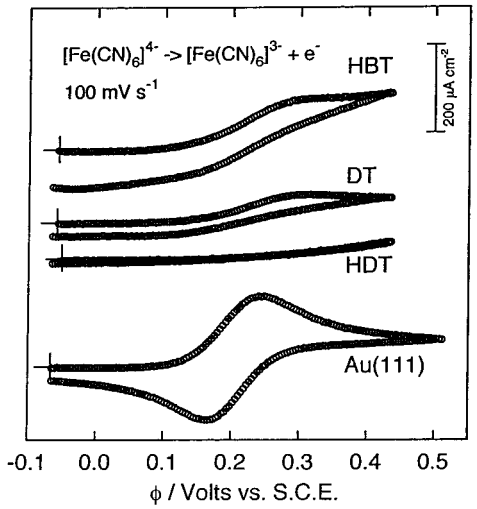

Figure 3. Cyclic voltammograms for the oxidation of 1 mM $[Fe(CN)_6]^{4-}$ in 0.5 M $NaClO_4$ at a Au(111) electrode and Au(111) SAM-modified electrodes. The scan rate was 100 mV s^{-1}. The symbol + indicates the potential where the cycle was started and current was zero.

and reduction peaks are distorted, and the double-layer region is altered when the electrode is of poor quality. Figure 2 shows a typical cyclic voltammogram of Au(111) in 0.01 M $HClO_4$ displaying the oxidation and reduction of the gold surface and the electrolyte. The potential of zero charge (pzc) has the value of 0.230 V against the SCE with a capacity of 20 μF cm^{-2} for Au(111) in 0.01 M $HClO_4$. $NaClO_4$ was chosen as the electrolyte because of concern that $HClO_4$ at low pH might complicate the data interpretation. If the hydroxyl groups of the SAM were protonated in low-pH solvents, a complicated double-layer region would result. Therefore, the Au(111) baseline was determined in $NaClO_4$ and is shown in Figure 2. The pzc of Au(111) in 0.01 M $NaClO_4$ is similar to the pzc in $HClO_4$. However, the oxidation and reduction peaks are broadened in $NaClO_4$.

Figure 3 shows cyclic voltammograms of Au(111) and Au(111) modified with a SAM in the presence of 1 mM $Na_4[Fe(CN)_6]$ in 0.5 M $NaClO_4$. The scan rate was in the positive direction at 100 mV s^{-1}. The bottom plot shows the oxidation of ferrocyanide to ferricyanide on Au(111). The formal potential is 0.230 V against the SCE and was calculated from the mean value of the peak potentials. It was observed that the splitting of the peak potentials was 75 mV for scan rates less than 200 mV s^{-1}. These data for Au(111) are consistent with a quasi-reversible electron-transfer model. When the electrode is modified with a SAM, a noticeable decrease in the peak current is observed in the cyclic voltammogram as well as an increase in the splitting of the peak potentials and a tendency of the voltammogram to adopt a sigmoidal line shape. These observations are in agreement with those obtained for ultramicroelectrodes and indicate that the electron-transfer reaction might be occurring at pinhole sites.[4] The CV for bare Au(111) is a prototypical example of planar diffusion to the electrode surface. The greatest decrease in the peak current occurs for HDT-modified Au(111) while DT- and HMB-modified electrodes allow a modest amount of electron transfer to occur, in comparison.

Impedance Spectroscopy. The impedance of three SAM-modified Au(111) electrodes was measured and compared to the case of bare Au(111). Systems of quite different properties were chosen, including decanethiol (DT), which has been studied extensively,[4,16,17,22] ω-hydroxydecanethiol (HDT),[3,20,21] and 4′-hydroxy-4-mercaptobiphenyl (HMB), a new system. Our purpose was to compare a conjugated biphenyl system with an alkanethiol.

There are several methods used to analyze impedance data. The data here are presented in the complex plane, a plot of $-Z''$ versus Z', or Argand space, with $-Z''$ so that the data appear in the first quadrant of the Cartesian plane. $-Z''$ and Z' are parametric functions of ω. The aim of this work is to generate an equivalent circuit, based upon an intuitive understanding of the physical situation at hand, as warranted by the empirical data. From the equivalent circuit model it is possible to write down algebraic equations for the $-Z''$ and Z' and fit the experimental data, in the complex plane, to obtain the magnitude of the ideal circuit elements. Finally, the ideal circuit elements are related to microscopic chemical processes occurring during the experiment.

Figure 4 shows the results of impedance spectroscopy on Au(111) and Au(111) modified with DT, HDT, and HMB in the presence of equimolar (1 mM) $[Fe(CN)_6]^{4-/3-}$ and 0.5 M $NaClO_4$ measured at the formal potential. The system comprised of bare Au(111) is shown in plot A and is described quite well by the Randles circuit in Figure 1. The results of the CNLS regression analysis are plotted as a solid curve with the values of the circuit elements given in Table 1.

The semicircle located near the origin is probed by higher frequencies than the linear region located to the right in plot A. The top of the semicircle corresponds to the frequency

$$\omega_p = \frac{1}{(R_{CT}C_{DL})} \tag{7}$$

The charge-transfer resistance for $[Fe(CN)_6]^{4-/3-}$ and the double-layer capacity for this system were 24.4 ± 0.3 Ω cm^2 and 20.9 ± 0.6 μF cm^{-2}, respectively. Therefore, ω_p

(16) Ulman, A. *An Introduction to Ultrathin Organic Films*; Academic Press: New York, 1991; and references therein.
(17) Chidsey, C. E. D.; Loiacono, D. N. *Langmuir* **1990**, *6*, 682−691.
(18) Cheng, J.; Saghi-Szabo, G.; Tossell, J. A.; Miller, C. J. *J. Am. Chem. Soc.* **1996**, *118*, 680−684.
(19) Fawcett, W. R.; Kovacova, Z.; Motheo, A. J.; Foss, C. A., Jr. *J. Electroanal. Chem.* **1992**, *326*, 91.
(20) Miller, C. J.; Gratzel, M. *J. Phys. Chem.* **1991**, *95*, 5225−5233.
(21) Becka, A. M.; Miller, C. J. *J. Phys. Chem.* **1993**, *97*, 6233−6239.
(22) Creager, S. E.; Steiger, C. *Langmuir* **1995**, *11*, 1852−1854.

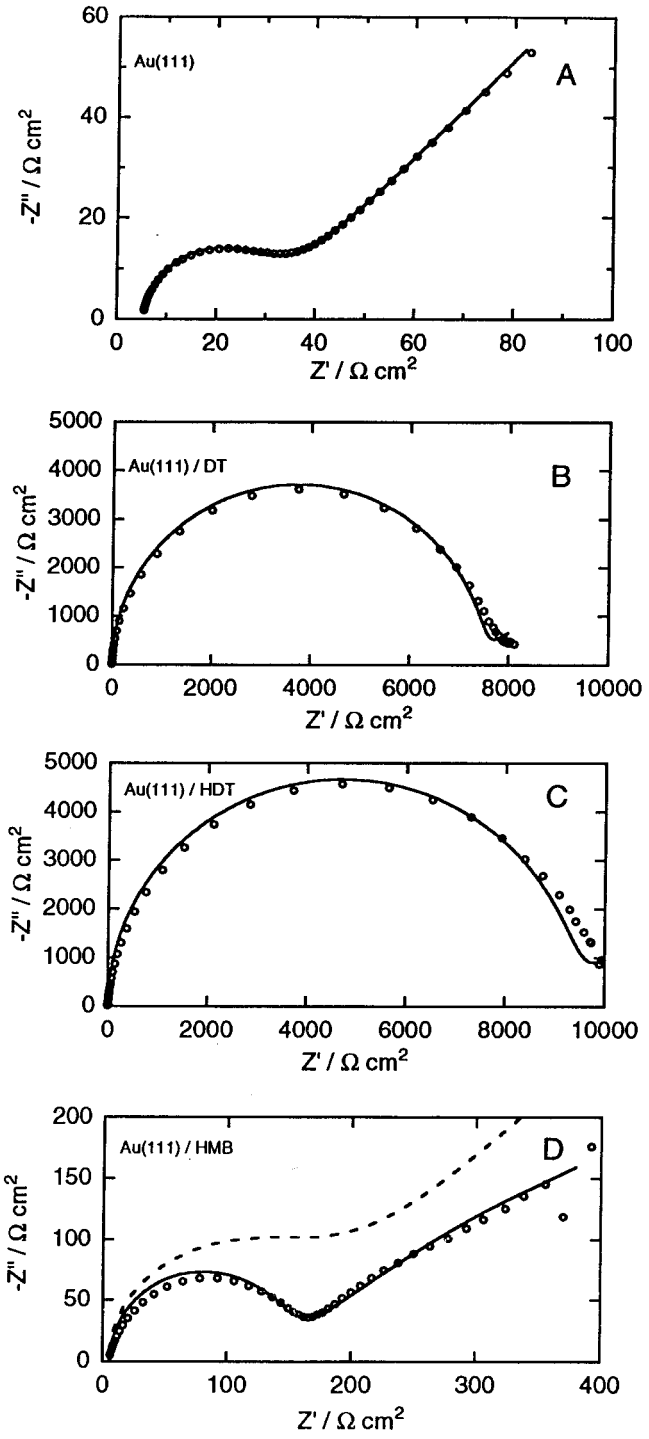

Figure 4. Argand space plots of the impedance of (A) Au(111) in the presence of 1 mM $[Fe(CN)_6]^{4-}$ and 1 mM $[Fe(CN)_6]^{3-}$ with 0.5 M $NaClO_4$ as the supporting electrolyte, (B) Au(111) modified with DT, (C) Au(111) modified with HDT, and (D) Au(111) modified with HMB; the dashed line is the best CNLS regression to the Randles circuit model. The electrode potential was 0.230 V against a SCE: (○) experimental data; (—) fit to equivalent circuit model using CNLS regression. The frequency range was 1 Hz to 10 kHz.

is approximately 1960 rad s^{-1} (ν = 312 Hz). In this frequency range the dynamics of electron transfer are observed in the impedance spectroscopy experiment and the current due to voltage excitation is under kinetic control. The low-frequency region of plot A, where the slope of $-Z''$ versus Z' is unity, is dominated by mass transfer of the redox species to and from the interfacial region. The slope of the frequency dependence of the Warburg impedance is 133 Ω $s^{-1/2}$ cm^2, which yields a diffusion coefficient of 0.8×10^{-5} cm^2 s^{-1}. The fact that the Argand plot has a unit slope in this region is readily seen by using equal scales for the abscissa and the ordinate. The high-frequency Z' intercept is the locus of the solution resistance. In this study the capacitance was modeled as an ideal capacitor in the circuit model. However, it is known that the capacity of solid electrodes shows a marked power law dependence or constant phase element (CPE).[19] This effect would be observed as a depressed semicircle in the complex plane. The CPE effect was verified in the present experiments; however, it has a negligible effect for these systems, so that the Au/solution interface can be represented as a simple capacitor as a first-order approximation.

The results for the decanethiol-coated Au(111) in the presence of the electron-transfer reaction are shown in plot B of Figure 4. In the case of DT/Au(111) the low-frequency linear-mass-transfer region is not observed because the reaction is under kinetic control over the entire frequency range; in other words the current is not limited by mass transfer at any frequency in the range studied. The charge-transfer resistance increases to 7396 ± 132 Ω cm^2, and the double-layer capacity drops to 1.49 ± 0.13 μF cm^{-2}. These data are consistent with the cyclic voltammetry experiment, which shows that DT inhibits electron transfer. When the electrode is covered with ω-hydroxydecanethiol, a further increase is observed in the charge-transfer resistance, indicating that the facility of the electron transfer reaction is markedly reduced. The charge-transfer resistance increased by 25% to 9239 ± 201 Ω cm^2, and the interfacial capacity was 2.57 ± 0.07 μF cm^{-2}. The Randles circuit was used as a model for both the DT- and HDT-modified electrodes. The capacities are consistent with previously observed[3−5,17,20,21,22] values in aqueous electrolytes. The data in plots B and C of Figure 4 exhibited a larger standard deviation in the low-frequency range, and therefore the CNLS fit was weighted to higher frequencies.

Plot D of Figure 4 shows the impedance spectrum of Au(111) modified by the biphenylthiol HMB in the presence of equimolar $[Fe(CN)_6]^{4-/3-}$ and 0.5 M $NaClO_4$. The charge-transfer resistance has decreased from that observed for DT- and HDT-modified gold, indicating that HMB is a poor barrier to electron transfer compared to the SAMs involving straight chain alkanethiols. Although the data in plot D resemble those in plot A, there are some very important differences. The slope of the low-frequency region for Au(111) modified by HMB is not unity and indicates that a Randles circuit is not appropriate for this system. If one assumes the Randles model for this system, it is impossible to model correctly the charge-transfer data. To resolve the equivalent circuit in greater detail, the impedance of Au(111)/HMB was measured in the absence of the ferrocyanide/ferricyanide redox couple in the same electrolyte, the results being shown in Figure 5. The results demonstrate that the non-Faradaic impedance consists of a large interfacial resistance in parallel with the double-layer capacitance. The parallel interfacial resistance is designated as R_{SAM} in Figure 1 and must be added to the circuit description in order to obtain a fit to the experimental data. If the SAM were behaving as an ideal capacitor, then one would observe a vertical line in the complex plane with a Z' high-frequency intercept equal to the solution resistance and $-Z'' = 1/(C\omega)$, where C is the capacity of the film. Clearly Figure 5 demonstrates more complex behavior and suggests that the parallel resistance is due to mobile charges flowing in the region of the SAM.

Table 1. CNLS Regression Results[a]

	R_s/Ω cm^2	R_{CT}/Ω cm^2	C_{DL}/μF cm^{-2}	σ/Ω s$^{-1/2}$ cm^2	R_{SAM}/Ω cm^2
Au(111)	5.72 (0.27)	24.43 (0.32)	20.9 (0.64)	133.3 (0.92)	
Au(111)/DT	5.69 (0.19)	7396 (132)	1.49 (0.13)	498 (368)	
Au(111)/HDT	5.91 (0.31)	9239 (201)	2.57 (0.07)	663 (492)	
Au(111)/HBT	4.46 (0.85)	158.8 (1.36)	4.46 (0.09)	330 (43)	1179 (46)

[a] The circuit elements are shown in Figure 1; R_{CT} and σ and σ are defined in eqs 4 and 5.

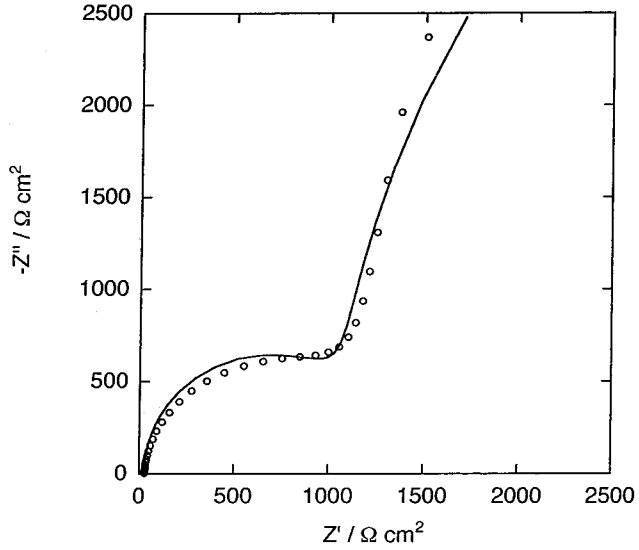

Figure 5. Argand space plots of the impedance of Au(111) modified with HMB in 0.5 M $NaClO_4$ showing a large interfacial resistance in parallel with the capacity due to the SAM. The electrode potential was 0.230 V against the SCE: (○) experimental data; (—) fit to equivalent circuit model using CNLS regression. The frequency range was 1 Hz to 10 kHz.

Further experiments to determine the nature of R_{SAM} indicate that R_{SAM} is dependent on the size of the cation of the inert electrolyte and the electrode potential. This resistance due to the movement of ions in and out of the SAM film is quite separate from the charge-transfer resistance, which describes the flow of charge across the modified interface into the electrode. It is reasonable to include it as a parallel component to the charge-transfer resistance of the redox couple in solution. The total model circuit then gives a good description of the impedance data.

The algebraic equations for the ideal circuit in the HMB system are more complicated than those for the Randles model. Figure 1 shows the general arrangement of elements corresponding to a circuit that will fit the complete data set. The Randles terms are shown in the dotted boxes with microscopic interpretations as described above. The presence of a large interfacial resistance, R_{SAM}, is included in parallel with the interfacial capacitance, C_{DL}. There are also terms for the stray capacitance of the system and the uncompensated resistance, which are present in any electrochemical experiment and which are observed at low electrolyte concentrations or in systems which have large solution resistances. However, it should be stressed that the contribution from R_U and C_{stray} was negligible in the systems studied here.

If one considers this new model for the Faradaic impedance of self-assembled monolayers, then

$$Z_T(j\omega) = \left(\frac{1}{Z_{RN}} + \frac{1}{Z_{SAM}}\right)^{-1} + Z_{SN} + Z_{stray} \qquad (8)$$

where Z_{RN} is given by eqs 2 and 3, Z_{SAM} is equal to R_{SAM}, Z_{SN} is the solution resistance, and Z_{stray} is the impedance of the stray capacitance. This model was used to fit the data for Au(111) modified by HMB shown in plot D of Figure 5. The results of the regression are shown in Table 1 and indicate that the charge-transfer resistance has decreased to 158.8 Ω cm^2, the double-layer capacitance is 4.46 μF cm^{-2}, and the interfacial resistance R_{SAM} is 1179 Ω cm^2.

The impedance spectroscopy data agree qualitatively with the observed cyclic voltammograms. It is tempting to relate the peak current in the cyclic voltammogram and the magnitude of the charge-transfer resistance to the coverage of the electrode by assuming that electron-transfer reactions occur only at bare spots on the electrode surface and that diffusion to these defect sites is planar. If the above assumption is correct, then one may assume an equation for the apparent fractional coverage of the electrode based on the peak current and the charge-transfer resistance of the uncoated electrode

$$\theta^R_{IS} = 1 - \left(\frac{R^{bare}_{CT}}{R^{SAM}_{CT}}\right) \qquad (9)$$

and

$$\theta^i_{CV} = 1 - \left(\frac{i^{bare}_p}{i^{SAM}_p}\right) \qquad (10)$$

The values for θ^P_{CV} are qualitatively similar to the trend in θ^i_{IS}; however, the magnitude of the cyclic voltammetric fractional coverages is always less than the fractional coverages obtained from the impedance spectroscopy data. However, previous work[23,24] has demonstrated that eq 10 is inappropriate for describing the fractional coverage because of the dominance of radial diffusion near each defect site. In both cases the HDT-modified electrode inhibits electron transfer more than DT and HMB. If the assumption that charge transfer occurs at bare spaces in the SAM holds, then it may be concluded that HDT forms better monolayers than DT and HMB. In addition to this method of estimating the fractional coverage, one may also consider another technique based on an analysis of pore size distribution in the SAM. The discrepancy in the fractional coverage estimates is explained better if radial diffusion to the micropores in the SAM film dominates. Finklea et al.[4] have established that, if radial diffusion to micropores is occurring, then the peak current observed is not a simple function of the exposed area of the SAM-coated electrode. One must also consider the distribution and radial size of the pores to adequately describe the surface structure and its effect on electron transfer.

Finklea et al.[4] have measured the Faradaic impedance of gold electrodes modified with octadecanethiol in 0.5 M H_2SO_4. A model based on the work of Matsuda[23] and Amatore[24] was developed to fit the Faradaic impedance

(23) Tokuda, K.; Gueshi, T.; Matsuda, H. *J. Electroanal. Chem.* **1979**, *102*, 41−48.
(24) Amatore, C.; Saveant, J. M.; Tessler, D. J. *J. Electroanal. Chem.* **1983**, *147*, 39−51.

data for charge-transfer reactions at perforated SAM-coated electrodes in order to understand the nature of the pores in SAMs. The expressions for the Faradaic impedance of a microporous SAM in the limit of high frequency are

$$Z'_f(\omega) = \frac{R_{CT}}{(1-\theta)} + \frac{\sigma}{\sqrt{\omega}} + \frac{\sigma}{[(1-\theta)\sqrt{\omega}]} \qquad (11)$$

and

$$Z''_f(\omega) = \frac{\sigma}{\sqrt{\omega}} + \frac{\sigma}{[(1-\theta)\sqrt{\omega}]} \qquad (12)$$

and in the low-frequency limit, they are

$$Z'_f(\omega) = \frac{R_{CT}}{(1-\theta)} + \frac{\sigma}{\sqrt{\omega}} + \frac{\sigma r_a (0.72D)^{1/2}}{(1-\theta)} \qquad (13)$$

and

$$Z''_f(\omega) = \frac{\sigma}{\sqrt{\omega}} \qquad (14)$$

In eq 13 r_a is the radius of the pore. These results show how the observed impedance is related to pore size and fractional coverage. One obtains the Faradaic impedance by subtracting the effects of the double-layer capacity and the solution resistance from the total impedance. The impedance associated with the double-layer capacity ($1/j\omega C_{DL}$) must be subtracted in the admittance representation while the solution resistance can be eliminated using the impedance coordinates.

The solution resistance is obtained by measuring the impedance of the system at very high frequencies, that is >10 kHz, in the presence or absence of the redox couple. The preferred method is to measure the solution resistance in each experiment in the presence of the redox couple because variations of electrode placement from trial to trial will affect the magnitude of the solution resistance. In the limit of high frequency the effects of capacitance and charge-transfer resistance (see eqs 2 and 3) are minimized and the real component of the impedance is equal to the solution resistance. Typical values in this work are approximately 5.5 Ω cm^2.

Measurement of the interfacial capacitance is a more complex matter. Some workers[4,23] have assumed that the capacitance measured in the absence of the charge-transfer couple is equal to the capacity in the presence of the reaction; they subtract this quantity from the electrode admittance to obtain the Faradaic impedance. Otherwise one may measure the impedance of the complete system in the presence of the Faradaic reaction and use the value of the double-layer capacity obtained in an analysis of these data to estimate the Faradaic impedance. The latter method was chosen in this study. It was noted that the capacities of all electrodes in the absence of the Faradaic reaction were similar to those obtained in the presence of the charge-transfer couple.

The real Faradaic impedance Z'_f of the four systems under study is presented in Figure 6. The subtraction procedure does increase the level of noise in the data, but meaningful information is indeed still present. Plot A (bare Au(111)) shows that Z'_f varies linearly with $\omega^{-1/2}$ with a *y*-intercept equal to the charge-transfer resistance and a slope corresponding to the value σ in eq 6. The mass-transfer parameter, namely, the diffusion coefficient,

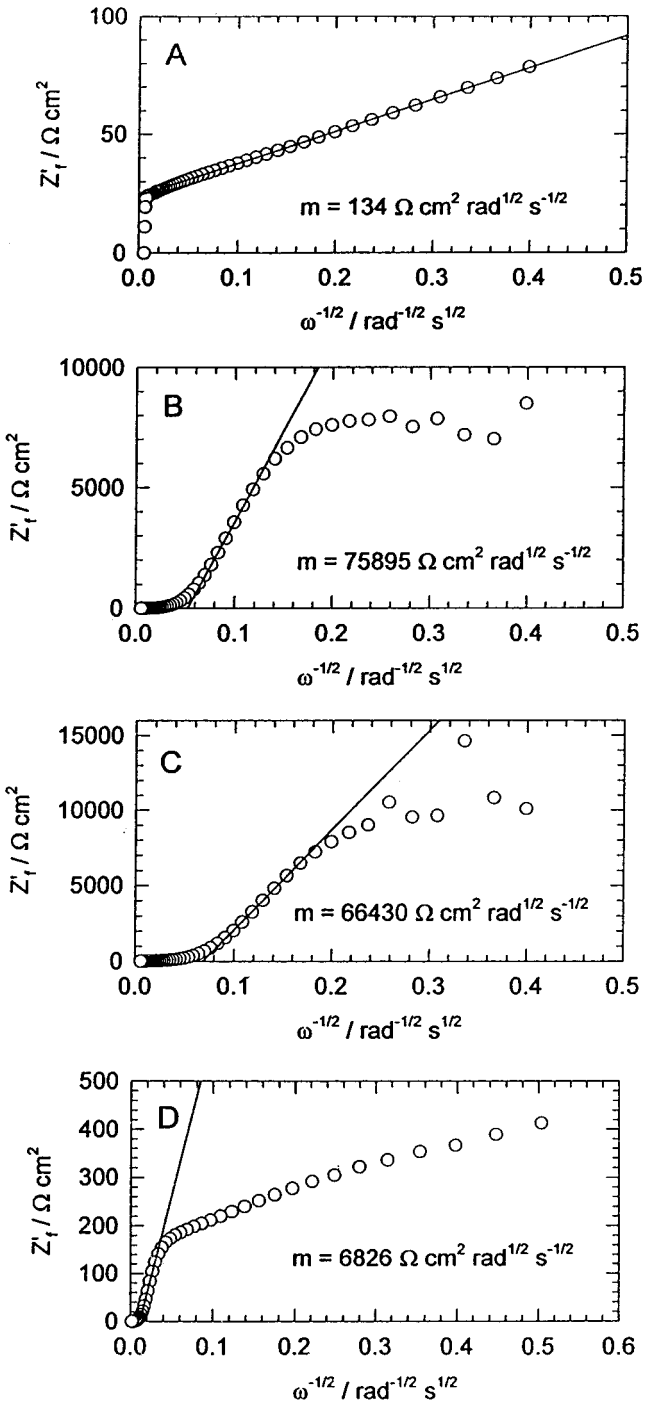

Figure 6. Real part of the Faradaic impedance plotted as a function of $\omega^{-1/2}$ and corresponding linear regression to the low-frequency region of the curve to obtain the slope *m*: (A) Au(111) in the presence of 1 mM $[Fe(CN)_6]^{4-}$ and 1 mM $[Fe(CN)_6]^{3-}$ with 0.5 M $NaClO_4$ as the supporting electrolyte; (B) Au(111) modified with DT; (C) Au(111) modified with HDT; (D) Au(111) modified with HMB. The electrode potential was 0.230 V against the SCE. The solution resistance and interfacial capacity have been subtracted for each case using the data in Table 1.

is available from the slopes of the lines shown in Figure 6. The subsequent diagrams in Figure 6 for SAM-modified Au(111) are qualitatively different due to the presence of the monolayer. These data support the hypothesis that electron transfer may occur through pores in the SAM structure and may be described, at least qualitatively, by the model involving a distribution of pores.

Table 2. Apparent Fractional Electrode Coverage

	θ^{R}_{IS}	θ^{i}_{CV}	θ^{P}_{IS}
Au(111)	0	0	0
Au(111)/DT	0.9967	0.5968	0.9980
Au(111)/HDT	0.9974	0.7586	0.9980
Au(111)/HMB	0.8462	0.4912	0.9974

A closer examination of eqs 11−14 reveals that the slope of the high-frequency region for plots shown in Figure 6 is

$$m = \sigma + \frac{\sigma}{(1 - \theta)} \tag{15}$$

Therefore, if σ is known from the experiment involving unmodified Au(111), it is possible to compute the fractional electrode coverage θ from the slope. This was done for the three SAMs considered in this study. The results are presented in Table 2 along with the values of θ calculated from CV and from IS using the ratio of the charge-transfer resistance.

It is interesting to compare the fractional coverage values obtained using the different techniques. By examining Table 2, it is clear that the qualitative trends of the estimates of the fractional coverage are similar between the three methods. However, there is some difference in the magnitude of the θ values. The lowest estimates for θ are obtained by cyclic voltammetry, where the peak current of the unmodified electrode is compared with the peak currents of the SAM-coated systems, assuming planar diffusion. This is most likely due to the dominance of spherical diffusion to defect sites in the SAM. The θ values calculated from impedance spectroscopy, both by using the values of the charge-transfer resistance and by using the method of Finklea,[4] are similar in magnitude, but the fractional coverage by the pore size model[4,23,24] tends to overestimate the area covered by the SAM. This may be due to nonidealities, such as assumptions regarding the geometry of the pores, that are pointed out by Finklea and also due to the uncertainty of the slope values because of the noisy nature of this numerical subtraction. The best way to estimate the fractional coverage seems to be by measuring the charge-transfer resistance in the presence of the SAM and comparing these values with those for an electrode that is unmodified. The charge-transfer resistance is relatively easy to identify by impedance spectroscopy, but it must be stressed that the circuit model used in the analysis requires verification, as shown in this study.

Conclusions

The impedance spectroscopy of Au(111) modified by decanethiol, ω-hydroxydecanethiol, and 4′-hydroxy-4-mercaptobiphenyl can be measured in the presence of 1 mM $[Fe(CN)_6]^{4-/3-}$. The Randles circuit has been used to fit the simplest impedance spectrum for some SAM-modified solid electrodes, but this work shows that the Randles model is not the best choice for all systems. One must verify the equivalent circuit in the absence of the redox couple over a wide frequency range before results in the presence of electron transfer are analyzed. This study shows that in the case of SAMs composed of hydroxy-terminated biphenyl monomers a large interfacial resistance is present along with the double-layer capacity and the charge-transfer resistance. This result is interesting because the conjugated π-electron system of the biphenyl ring may be promoting electron transfer through the thin SAM on the electrode. However, because electron transfer is also occurring at defect sites in the SAM which expose the bare electrode, the separation of through-bond tunneling from radial diffusion to the metal surface is not possible. An ideal method for studying through-bond tunneling would be to fix the redox couple at the end of the thiol spacer group. The fact the Randles model is not valid for the 4′-hydroxy-4-mercaptobiphenyl system contradicts the idea that all SAMs can be modeled as simple dielectric materials coating the electrode surface. The observed interfacial resistance may be due to reorientation of dipoles in the SAM structure or due to solvent/ion permeation into the bulk of the SAM. Spectroscopic studies are underway in this laboratory to elucidate the nature of the parallel resistance.

In addition to clarifying the equivalent circuit used to model the impedance of electrodes modified with self-assembled monolayers, this study has estimated the fractional SAM coverage θ by several methods. A discrepancy was observed among the θ values for SAMs estimated by the decrement in the charge-transfer resistance, from the CV peak current density ratio, and by using the pore size distribution model of Finklea. The fractional coverage θ estimated from the CV peak current was quantitatively very different from values obtained by other methods. The observed discrepancy in fractional coverage is in support of earlier work by Matsuda[23] and Amatore,[24] who have established that because of the nature of the distribution of defect sites a simple current ratio calculation as implied by eq 10 is not appropriate. To estimate accurately the fractional coverage of a SAM-coated electrode, a more sophisticated model is required; with such a model cyclic voltammetry can be used to estimate the fractional electrode coverage.

The charge-transfer resistance was greatest for ω-hydroxydecanethiol SAMs compared to the decanethiol and 4′-hydroxy-4-mercaptobiphenyl systems. 4′-Hydroxy-4-mercaptobiphenyl self-assembled monolayers do not strongly inhibit electron transfer for a solution-phase redox species and may in fact promote electron transfer due to the delocalized π-electrons of the biphenyl ring.

Acknowledgment. We wish to acknowledge helpful discussions with Professors Zofia Borkowska and Cary Miller. Financial support by the National Science Foundation through Grant number CHE-94-11659 is also gratefully acknowledged.

LA970980+